

Multiple Topological Magnetism in van der Waals Heterostructure of MnTe₂/ZrS₂

Zhonglin He, Kaiying Dou, Wenhui Du, Ying Dai*, Baibiao Huang, Yandong Ma*

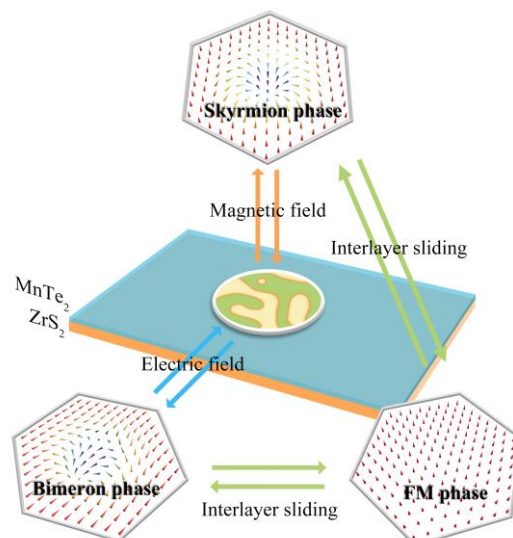
School of Physics, State Key Laboratory of Crystal Materials, Shandong University, Shandan Street 27, Jinan 250100, China

*Corresponding authors: daiy60@sdu.edu.cn (Y.D.); yandong.ma@sdu.edu.cn (Y.M.)

Abstract

Topological magnetism in low-dimensional systems is of fundamental and practical importance in condensed-matter physics and material science. Here, using first-principles and Monte-Carlo simulations, we present that multiple topological magnetism (i.e., skyrmion and bimeron) can survive in van der Waals Heterostructure of MnTe₂/ZrS₂. Arising from interlayer coupling, MnTe₂/ZrS₂ can harbor a large Dzyaloshinskii-Moriya interaction. This, combined with ferromagnetic exchange interaction, yields an intriguing skyrmion phase consisting of sub-10 nm magnetic skyrmions under a tiny magnetic field of ~ 75 mT. Meanwhile, upon harnessing a small electric field, magnetic bimeron can be observed in MnTe₂/ZrS₂ as well, suggesting the existence of multiple topological magnetism. Through interlayer sliding, both topological spin textures can be switched on-off, suggesting their stacking-dependent character. In addition, the impacts of d_{\parallel} and K_{eff} on these spin textures are revealed, and a dimensionless parameter κ is utilized to describe their joint effect. These explored phenomena and insights not only are useful for fundamental research in topological magnetism, but also enable novel applications in nanodevices.

Keywords: skyrmion, bimeron, first-principles, Dzyalohinskii-Moriya interaction, heterostructure



Introduction

Since the first experimental observations of skyrmion lattice in bulk MnSi [1] and Fe_{0.5}Co_{0.5}Si thin films [2], magnetic skyrmion, a typical topological magnetism, has been a prominent topic of condensed matter physics [3,4]. It is a spatially localized topological spin structure that is homotopically equivalent to a unit sphere, and characterized by quantized topological charge $Q = \pm 1$ [5]. Such non-trivial topological nature ensures an exceptional stability in terms of transition into trivial spin textures [e.g., ferromagnetic (FM) phase], making it technologically appealing for future memory and computing devices [6-8]. In addition to the study of magnetic skyrmions in perpendicularly magnetized systems, there has also been much effort in searching for new forms of topological magnetism in in-plane magnetized systems. One promising example is magnetic bimeron, which consists of a pair of merons and is of great interest recently because of its extraordinary properties [9,10]. In principle, magnetic bimeron is related to magnetic skyrmion with a $\pi/2$ -rotation of each spin around in-plane axis [11]. As the topological charge Q is invariant under such rotation [5], magnetic bimeron exhibits topological nature and inherent stability as well [10].

The demand for device miniaturization in modern electronics stimulates the exploration of topological magnetism in two-dimensional (2D) materials [12,13]. The essential ingredient for the realization of topological magnetism is the Dzyaloshinskii-Moriya interaction (DMI) that exists under broken inversion symmetry and strong spin-orbit coupling (SOC). DMI is a form of antisymmetric exchange interaction, establishing a preferred chirality for spin textures [14-16]. In the past years, for realizing large DMI in 2D systems, extensive efforts have been devoted to Janus and ferroelectric structures [17,18]. While the former requires harsh conditions to realize in experiment [19,20], the latter severely limits the materials choices [21]. As a result, only a few 2D candidate systems have been proposed so far [16,18,22-25]. New and general mechanism for topological magnetism formation is highly desired for its exploration in the emerging area of 2D magnets. We also note that DMI can be induced in 2D van der Waals heterostructure (vdWH) [12], and superior to Janus and ferroelectric systems, vdWH systems exhibit higher experimental feasibility and tunability, providing an ideal platform for topological magnetism research. Nonetheless, the formation of topological magnetism in 2D vdWH is rarely reported [26,27], as the DMI is usually too weak to stabilize topological spin textures.

Here, through first-principles calculations and Monte-Carlo (MC) simulations, we propose the existence of multiple topological magnetism (i.e., skyrmion and bimeron) in 2D MnTe₂/ZrS₂ vdWH. Due to the strong interlayer interplay, MnTe₂/ZrS₂ possesses a large DMI. This, along with FM exchange interaction, results in the isolated zero-field magnetic skyrmion intrinsically in MnTe₂/ZrS₂.

When applying a tiny magnetic field of ~ 75 mT, intriguing skyrmion phase consisting of sub-10 nm magnetic skyrmions occurs. On the other hand, by harnessing a small electric field, magnetic bimeron can be observed. This confirms the existence of long-sought multiple topological magnetism in $\text{MnTe}_2/\text{ZrS}_2$. Furthermore, under interlayer sliding, both topological spin textures can be switched off, which suggests their stacking-dependent nature. Additionally, the roles of d_{\parallel} and K_{eff} in the formation of these spin textures are unveiled, and a dimensionless parameter κ is utilized to characterize their joint effect. Our results greatly enrich the research of 2D topological magnetism.

Results and Discussion

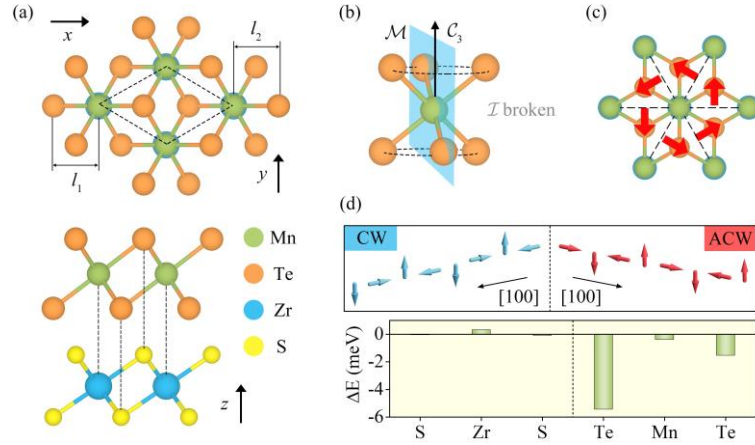


Fig. 1. (a) Top and side views of the crystal structure of $\text{MnTe}_2/\text{ZrS}_2$. The dashed diamond indicates the unit cell of $\text{MnTe}_2/\text{ZrS}_2$. (b) Distorted octahedral geometry of Mn atom. \mathcal{M} , \mathcal{I} and \mathcal{C}_3 represent the M -, I - and C_3 - symmetry, respectively. (c) DMI vectors \mathbf{D}_{ij} (red arrows) between the nearest-neighbor Mn atoms. (d) Two spin-spiral configurations of CW and ACW employed to obtain DMI parameters and atomic-layer-resolved localization of the DMI associated SOC energy ΔE for $\text{MnTe}_2/\text{ZrS}_2$.

$\text{MnTe}_2/\text{ZrS}_2$ vdWH is composed of two layers of MnTe_2 and ZrS_2 , which are known as FM metal and nonmagnetic semiconductor, respectively. These two constituent layers both belong to the 1T octahedral family of 2D transition metal dichalcogenides with space group $\text{P}\bar{3}\text{m}1$ (No. 164), thus exhibiting an inversion symmetry (I -symmetry). Obviously, when stacking these two layers together, I -symmetry is broken. Here, we consider three typical stacking patterns of $\text{MnTe}_2/\text{ZrS}_2$ [see **Fig. S1**], among which the AA stacking pattern shown in **Fig. 1(a)** is proved to be the most stable configuration. In the following, we only discuss the AA stacking pattern of $\text{MnTe}_2/\text{ZrS}_2$. $\text{MnTe}_2/\text{ZrS}_2$ exhibits a distorted octahedral geometry ($l_1 \neq l_2$) for Mn atoms, resulting in the space group $\text{P}3\text{m}1$ (No. 156). To

confirm the stability of MnTe₂/ZrS₂, we calculate its phonon spectra and perform ab initio molecular dynamics (AIMD) simulations. From **Fig. S2(a)**, we can see that all phonon branches are positive in the entire Brillouin zone, suggesting its dynamical stability. And as shown in **Fig. S2(b)**, after heating at 500 K for 5 ps, neither structure reconstruction nor bond breaking is found in MnTe₂/ZrS₂, confirming it is thermally stable.

Our calculations show that MnTe₂/ZrS₂ favors a spin-polarized state. The magnetic moment is calculated to be 3.35 μ_B per unit cell, which is mainly localized on Mn atom. For comparison, we also investigate the magnetic behavior of free-standing MnTe₂. The corresponding magnetic moment is calculated to be 3.23 μ_B per unit cell, which is in good agreement with the previous work [28]. To get further insight into the magnetic properties of MnTe₂/ZrS₂, we adopt the following atomically resolved Hamiltonian:

$$\begin{aligned}
H = & -J \sum_{\langle i,j \rangle} (\mathbf{S}_i \cdot \mathbf{S}_j) - \lambda \sum_{\langle i,j \rangle} (S_i^z \cdot S_j^z) - K_{CA} \sum_i (S_i^z)^2 \\
& - \frac{1}{2} \frac{\mu_0 g_0^2 \mu_B^2}{4} \sum_{\langle i,j \rangle} \frac{1}{r_{ij}^3} \left[\mathbf{S}_i \cdot \mathbf{S}_j - \frac{3}{r_{ij}^3} (\mathbf{S}_i \cdot \mathbf{r}_{ij})(\mathbf{S}_j \cdot \mathbf{r}_{ij}) \right] \\
& - \mu_{Mn} B \sum_i S_i^z - \sum_{\langle i,j \rangle} \mathbf{D}_{ij} \cdot (\mathbf{S}_i \times \mathbf{S}_j). \quad (1)
\end{aligned}$$

Here, \mathbf{S}_i is unit vector ($|\mathbf{S}_i| = 1$) indicating the local spin of i^{th} Mn atom. J represents the nearest-neighbor (NN) isotropic exchange interaction. λ and K_{CA} describe the NN anisotropic exchange interaction and magnetocrystalline anisotropy (MCA), respectively. The fourth term refers to the shape anisotropy K_{SA} . This, combined with K_{CA} , gives rise to an effective magnetic anisotropy $K_{\text{eff}} = K_{CA} + K_{SA}$. \mathbf{r}_{ij} is the vector from site i to j , μ_0 is the vacuum permeability, g_0 is the electron spin g -factor, and μ_B is the Bohr magneton. The penultimate term is Zeeman energy, where μ_{Mn} and B correspond to on-site magnetic moment of Mn atom and external magnetic field, respectively. \mathbf{D}_{ij} characterizes the DMI vector for each pair of NN Mn atoms.

To obtain the magnetic parameters of J , λ and K_{CA} , we consider four different spin configurations of a 2×1 supercell of MnTe₂/ZrS₂ shown in **Fig. S3**. The isotropic exchange parameter J is calculated to be 9.06 meV, which indicates a FM interaction between the NN Mn atoms. The underlying physics for such FM coupling in MnTe₂/ZrS₂ is associated with the Goodenough-Kanamori-Anderson rules [29-31]. In MnTe₂/ZrS₂, the Mn-Te-Mn bonding angle is 87°, approximately equal to 90°. According to the Goodenough-Kanamori-Anderson rules, the exchange coupling between NN Mn atoms is dominated by the superexchange interaction, leading to the FM coupling. This fact can also be

confirmed by the spin charge density of MnTe₂/ZrS₂ shown in **Fig. S6(a)**. It can be seen that aside from the dominated distribution of spin-up charge densities on Mn atoms, there are some spin-down charge densities distributed on the adjacent Te atoms, which suggests the superexchange interaction between NN Mn atoms.

The NN anisotropic exchange parameter λ is calculated to be 0.07 meV, which favors out-of-plane (OP) magnetization anisotropy. Besides λ , the easy magnetization axis (EMA) also relies on effective magnetic anisotropy K_{eff} , which, as mentioned above, contains two parts, i.e., magnetocrystalline anisotropy K_{CA} and shape anisotropy K_{SA} . For 2D magnetic materials, K_{SA} is only associated with the locations and magnetic moments of magnetic atoms, and usually prefers in-plane (IP) magnetization [32]. As expected, K_{SA} is calculated to be -0.13 meV for MnTe₂/ZrS₂. For K_{CA} , it is calculated to be 0.36 meV, yielding the effective magnetic anisotropy $K_{\text{eff}} = 0.23$ meV. Therefore, MnTe₂/ZrS₂ displays an OP EMA, and obviously, magnetocrystalline anisotropy plays a dominant role. To deeply understand this character, we investigate the underlying physics of OP magnetocrystalline anisotropy for MnTe₂/ZrS₂. Considering magnetocrystalline anisotropy is related to crystal field splitting and SOC, we introduce a perturbation theory of SOC effect, which can be written as [33]

$$\text{MCA} = \xi^2 \sum_{M,o,u,\sigma',\sigma} \sigma' \sigma \frac{|\langle u, \sigma | \hat{L}_z^M | o, \sigma' \rangle|^2 - |\langle u, \sigma | \hat{L}_x^M | o, \sigma' \rangle|^2}{E_{u,\sigma} - E_{o,\sigma'}}. \quad (2)$$

Here, u and o correspond to the unoccupied and occupied states of Mn atoms, respectively, $E_{u/o,\sigma}$ is the band energy of the state, and the spin indices σ and σ' run over ± 1 , referring to the two orthogonal spin states. M includes Mn and Te atoms. The positive (negative) value of MCA indicates OP (IP) magnetocrystalline anisotropy. **Fig. S4** presents the projected density of states for Mn- d orbitals of MnTe₂/ZrS₂. Clearly, both u and o are mainly contributed by $|d_{xz}/d_{yz}, \uparrow\rangle$ [\uparrow (\downarrow) represents spin up (down) states], which enforces $|\langle u, \sigma | \hat{L}_z^M | o, \sigma' \rangle|^2 \gg |\langle u, \sigma | \hat{L}_x^M | o, \sigma' \rangle|^2$. As a result, positive value of magnetocrystalline anisotropy is obtained, giving rise to the OP magnetocrystalline anisotropy for MnTe₂/ZrS₂.

We then investigate DMI in MnTe₂/ZrS₂, which plays a vital role in establishing topological magnetism. The space group P3m1 of MnTe₂/ZrS₂ includes three mirror symmetries (\mathbf{M} -symmetry) correlated by the three-fold rotation symmetry (\mathbf{C}_3 -symmetry) [**Fig. 1(b)**]. According to Moriya's rule [34], the DMI vector can be expressed as $\mathbf{D}_{ij} = d_{ij,\parallel}(\mathbf{u}_{ij} \times \mathbf{z}) + d_{ij,z}\mathbf{z}$, where \mathbf{u}_{ij} is the unit vector from site i to j , and \mathbf{z} is the OP unit vector. The two neighboring DMI of \mathbf{D}_{ij} and $\mathbf{D}_{i(j+1)}$ are related through \mathbf{M} -symmetry, i.e., $\mathbf{D}_{i(j+1)} = \det(\mathbf{M})\mathbf{M}\mathbf{D}_{ij}$, which indicates that $d_{i(j+1),\parallel} = d_{ij,\parallel} =$

d_{\parallel} and $d_{ij,z} = -d_{i(j+1),-z}$. This combined with C_3 -symmetry results in a toroidal arrangement of the IP DMI component $d_{ij,\parallel}$ [see **Fig. 1(c)**] and a staggered arrangement of the OP DMI component $d_{ij,z}$ for the six NN Mn atoms. Concerning the toroidal arrangement of $d_{ij,\parallel}$, it potentially tends to produce the Néel-type magnetic skyrmion. While for the staggered arrangement of $d_{ij,z}$, it would lead to the vanishing of the OP DMI component in average, making little contribution for stabilizing magnetic skyrmion [17,25]. Therefore, only d_{\parallel} is taken into consideration in the following. To obtain d_{\parallel} of MnTe₂/ZrS₂, we consider the clockwise (CW) and anticlockwise (ACW) spin-spiral configurations, as shown in **Fig. 1(d)**. Intriguingly, it has a large intrinsic DMI of $d_{\parallel} = -1.39$ meV.

For revealing the physical origin of such large DMI, the layer-resolved SOC energy difference ΔE between two spin-spiral configurations are calculated for isolated MnTe₂ and MnTe₂/ZrS₂. As shown in **Fig. S5** and **1(d)**, except for Te atomic layers, other atomic layers make minor contribution to DMI. This feature corresponds to the Fert-levy model [35]. For isolated MnTe₂, ΔE originated from two Te atomic layers are equal, but in opposite signs due to the protection of M -symmetry, leading to the vanishing DMI. In contrast, as shown in **Fig. S6(b)**, the strong electronic hybridization between the two layers in MnTe₂/ZrS₂ indicates a strong Te-S hopping, which results from large contact potential difference between MnTe₂ and ZrS₂ [**Fig. S6(c)**]. Apparently, the strong Te-S hopping has a significant impact on the lower Te atomic layer. That is to say, as illustrated in **Fig. 1(d)**, it inverses ΔE of the lower Te atomic layer, leading to the large DMI in MnTe₂/ZrS₂.

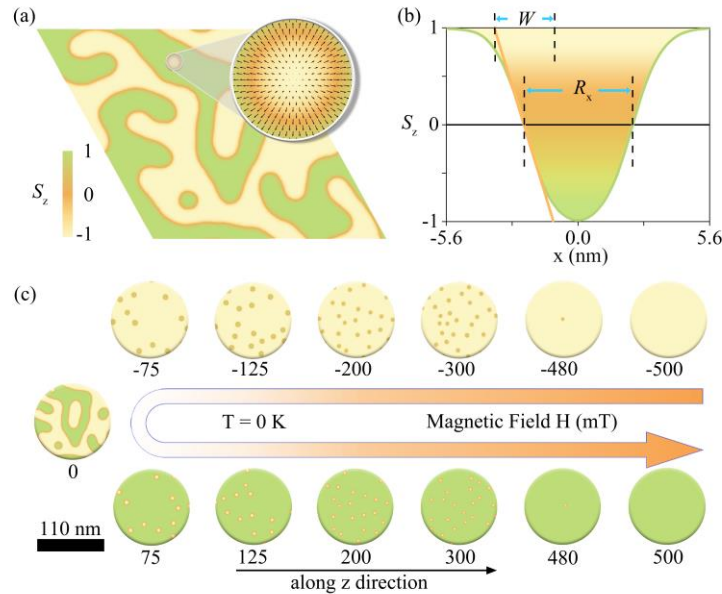


Fig. 2. (a) Spin texture of MnTe₂/ZrS₂ under zero-field. In (a), color map specifies the OP spin component and arrows indicates the IP spin component. (b) Line profiles of OP spin component along the central transect of magnetic skyrmion under magnetic field of ~ 75 mT. (c) Spin texture of

MnTe₂/ZrS₂ as a function of external magnetic field.

Based on the magnetic parameters obtained above, the absolute value of the ratio between DMI vector and NN isotropic exchange interaction is calculated to be $|d_{\parallel}/J| = 0.15$. We note that $|d_{\parallel}/J|$ is usually considered as a criterion for the formation of magnetic skyrmion [17,25]: for $|d_{\parallel}/J| > 0.1$, magnetic skyrmion tends to be stable; while for $0 < |d_{\parallel}/J| < 0.1$, it usually indicates a trivial magnetic state. In this regard, magnetic skyrmion might exist in MnTe₂/ZrS₂. To verify this possibility, we investigate the topological spin textures in MnTe₂/ZrS₂ based on the parallel tempering MC simulations. Here, we employ the topological charge Q to characterize the magnetic skyrmion, which can be expressed as [36]:

$$Q = \frac{1}{4\pi} \sum_n q_n, \quad (3)$$

with $\tan \frac{q_n}{2} = \frac{\mathbf{S}_i^n \cdot (\mathbf{S}_j^n \times \mathbf{S}_k^n)}{1 + \mathbf{S}_i^n \cdot \mathbf{S}_j^n + \mathbf{S}_j^n \cdot \mathbf{S}_k^n + \mathbf{S}_k^n \cdot \mathbf{S}_i^n}$. Here, \mathbf{S}_i^n , \mathbf{S}_j^n , \mathbf{S}_k^n are the three spin vectors of the n^{th} equilateral triangle in the anticlockwise lattice. **Fig. 2(a)** illustrates the spin textures of MnTe₂/ZrS₂. Obviously, a labyrinth domain pattern with Néel-type domain walls is observed. Along with these trivial patterns, intriguingly, a stabilized Néel-type magnetic skyrmion confirmed by $Q = \pm 1$ is also realized, without applying any external tuning.

We then investigate the evolution of spin texture of MnTe₂/ZrS₂ as a function of external magnetic field. As shown in **Fig. 2(c)**, the labyrinth domains shrink with increasing magnetic field, then disappear completely at a moderate magnetic field of ~ 75 mT. In this case, the Skyrmion phase is realized in MnTe₂/ZrS₂. More importantly, such phase is stable within a broad range of 75–480 mT. When further increasing the magnetic field, the Skyrmion phase is transformed into the trivial FM phase. **Fig. S7(a)** presents the radius of magnetic skyrmion as a function of magnetic field. It can be seen that the radius of magnetic skyrmion decreases with increasing the magnetic field from 0 to 75 mT. It is worthy emphasizing that the radius R_x of magnetic skyrmion for MnTe₂/ZrS₂ is only ~ 4.5 nm under 75 mT, and the wall width W is ~ 2 nm [see **Fig. 2(b)**]. With further increasing the magnetic field to 250 mT, the radius is almost unchanged. Upon increasing the magnetic field larger than 250 mT, the radius continues to decrease, and reduces to zero under 500 mT. In other words, all the Skyrmion phases in MnTe₂/ZrS₂ are composed of sub-10 nm magnetic skyrmions. Such a small size is highly promising for the practical applications in future skyrmionics devices. While for the density

of magnetic skyrmions, as illustrated in **Fig. S7(b)**, a maximum of $\sim 2 \times 10^{-3}$ per nm^2 (43 per supercell) is obtained under the magnetic field of 200-300 mT. By increasing the field further (300-480 mT), the density of magnetic skyrmion decreases rapidly, and suddenly shrinks to zero at 500 mT, corresponding to a quantum jump to the trivial FM phase.

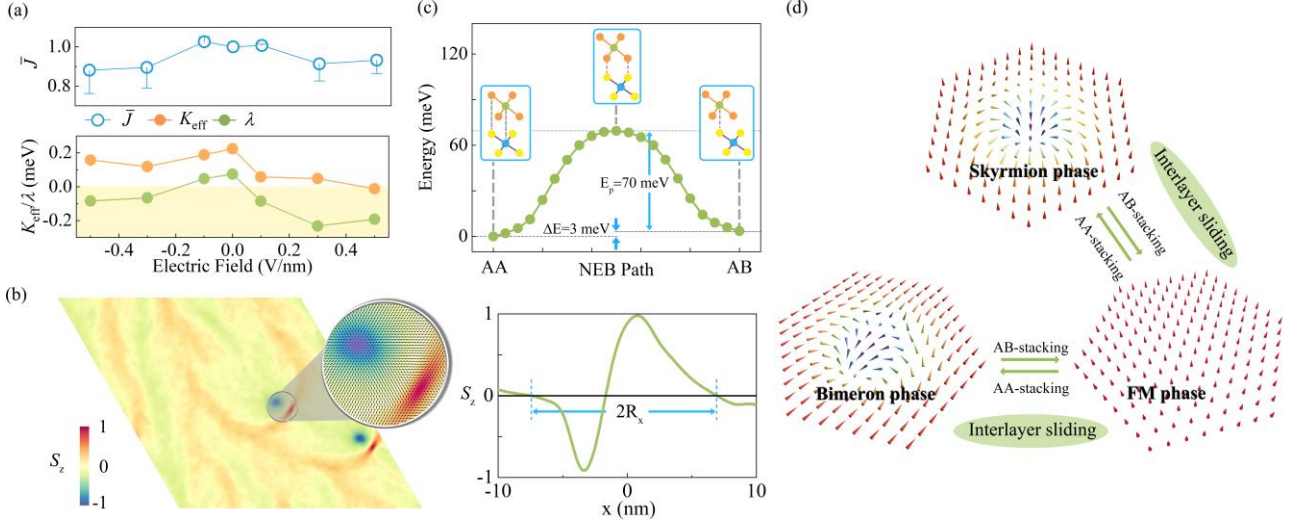


Fig. 3. (a) Magnetic parameters of $\text{MnTe}_2/\text{ZrS}_2$ as a function of applied electrical field. \bar{J} is the ratio between J under electric field and zero-field. (b) Spin texture of $\text{MnTe}_2/\text{ZrS}_2$ under electric field of 0.3 V/nm. Right panel in (b) illustrates the line profiles of OP spin component along the central transect of magnetic bimeron. In (b), color map specifies the OP spin component and arrows indicate the IP component. (c) Minimum energy path for interlayer sliding between AA and AB stacking patterns. (d) Schematic diagram of magnetic phase switching for $\text{MnTe}_2/\text{ZrS}_2$.

Similar to DMI, EMA, which is determined by λ and K_{eff} , is also of great importance for establishing the topological magnetism. As unveiled above, K_{eff} is sensitively depended on the electronic state around the Fermi level. In heterostructures, the electronic state can be easily manipulated via applying external electric field, which holds the possibility to tune K_{eff} as well as the topological magnetism. To this end, we investigate the effect of electric field on the topological spin textures of $\text{MnTe}_2/\text{ZrS}_2$. **Fig. 3(a)** shows the magnetic parameters of $\text{MnTe}_2/\text{ZrS}_2$ as functions of external electric field. It can be seen that, with increasing the electric field from -0.5 to 0.5 V/nm, J fluctuates in a narrow range, while λ and K_{eff} vary significantly. For the cases under electric field of -0.5 - 0.1 V/nm, the nature of OP EMA is preserved. Remarkably, when the electric field reaches 0.3 V/nm, the combined effect of λ and K_{CA} gives rise to an IP magnetization. The corresponding d_{\parallel} under 0.3 and 0.5 V/nm is calculated to be ~ 1.29 and 1.50 meV, respectively. This results in $\left| \frac{d_{\parallel}}{J} \right|$

=1.55 and 1.76, respectively, which might stabilize IP topological magnetism.

We then perform the parallel MC simulations to explore the spin textures of $\text{MnTe}_2/\text{ZrS}_2$ under the electric field of 0.3 and 0.5 V/nm. As shown in **Fig. 3(b)**, under the electric field of 0.3 V/nm, the magnetic bimeron with $Q = +1$ is observed in $\text{MnTe}_2/\text{ZrS}_2$. Inset of **Fig. 3(b)** presents the OP magnetization of magnetic bimeron as a function of the radial coordinate. The radius of magnetic bimeron R_x is ~ 14.3 nm, which is also suitable for practical application. We wish to point out that, in contrast to most of the previous work on bimeron [22,23,26], the magnetic bimeron achieved in $\text{MnTe}_2/\text{ZrS}_2$ is through electric field instead of magnetic field, indicating a more energy-saving way for exploring IP topological magnetism. When further increasing the electric field to 0.5 V/nm, as shown in **Fig. S8**, the magnetic bimeron still can be observed, but become vagueness, and the isolated merons emerge.

It is interesting to note that both DMI and EMA can be determined by interlayer hopping in $\text{MnTe}_2/\text{ZrS}_2$. And the interlayer hopping would be affected by the stacking pattern. Taking AB pattern as an example, we then discuss the effect of stacking pattern on the magnetic properties of $\text{MnTe}_2/\text{ZrS}_2$. The corresponding calculated magnetic parameters are summarized in **Table. S1**. And we obtain $\left|d_{\parallel}/J\right| = 0.069 < 0.1$, which implies a trivial FM phase. To confirm this behavior, we conduct the parallel MC simulations. **Fig. S9** shows the spin texture of AB stacked configuration. As is expected, it exhibits a trivial FM phase. This suggests that, by transforming $\text{MnTe}_2/\text{ZrS}_2$ from AA to AB stacking pattern through interlayer sliding, both magnetic skyrmion and bimeron would be destroyed. Once such interlayer sliding is feasible, as shown in **Fig. 3(d)**, the on-off switching of the topological magnetism can be achieved in $\text{MnTe}_2/\text{ZrS}_2$. **Fig. 3(c)** illustrates the minimum energy path for interlayer sliding between the stacking order of AA and AB. The energy barrier is estimated to be ~ 70 meV per unit cell, suggesting the feasibility of the interlayer sliding.

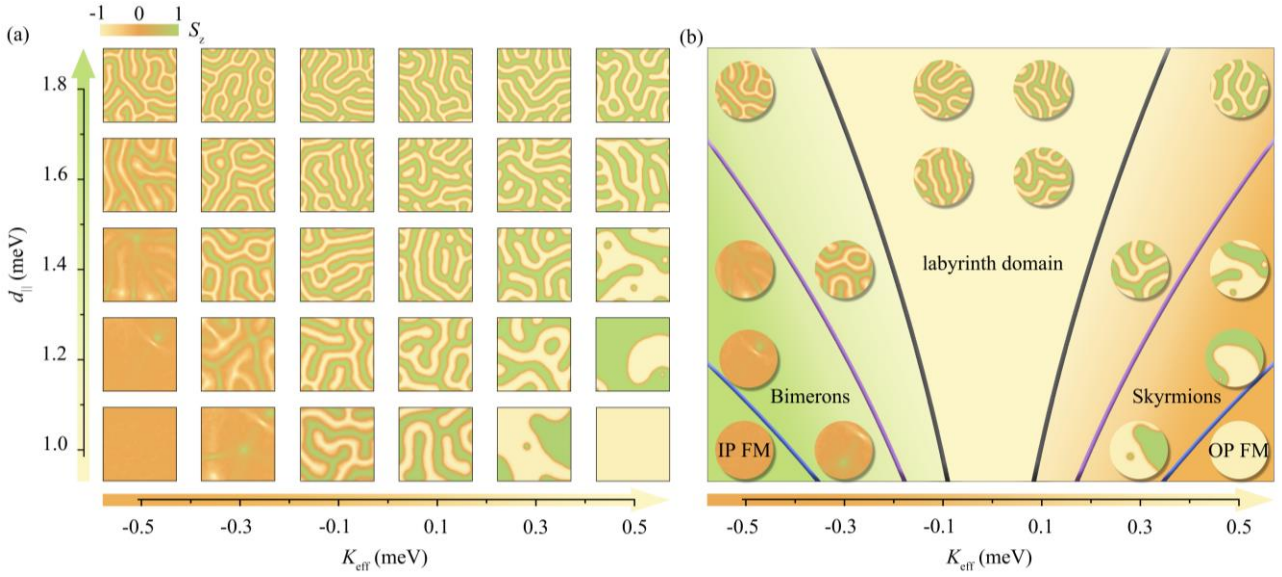


Fig. 4. (a) Spin texture diagram of $\text{MnTe}_2/\text{ZrS}_2$ as a function of d_{\parallel} and K_{eff} . J and λ are set to 9.06 and 0 meV, respectively. (b) Spin texture diagram of $\text{MnTe}_2/\text{ZrS}_2$ described by κ . In (b), the gray, purple and blue lines represent $\kappa = \pm 1$, $\kappa = \pm 2$ and $\kappa = \pm 4$, respectively. Color map specifies the OP spin component

At last, a phase diagram of the spin texture as a function of d_{\parallel} and K_{eff} is summarized in **Fig. 4(a)**. Since λ plays the same role as K_{eff} , we neglect the impact of λ , which is set to zero in MC simulations. As shown in **Fig. 4**, the trivial FM phase is observed under a small DMI and evolves into labyrinth domain phase with increasing DMI, which can shrink into Skyrmion phase upon introducing magnetic field. Therefore, a large DMI is essential for forming nontrivial topological spin textures. From **Fig. 4(a)**, with increasing DMI, we can also see that the density of labyrinth domain increases, and the size of labyrinth domain becomes smaller. Interestingly, arising from the large DMI, the magnetic skyrmions in $\text{MnTe}_2/\text{ZrS}_2$ would form a triangular lattice under magnetic field, leading to skyrmion crystal phase (**Fig. S10**). When modulating K_{eff} , as illustrated in **Fig. 4(a)**, the transition between the phases with magnetic skyrmion and bimeron can be observed. And the radius and density of magnetic skyrmion/bimeron are related to $|K_{\text{eff}}|$. Namely, a large $|K_{\text{eff}}|$ will introduce small density and radius of magnetic skyrmion/bimeron.

From above, we can see that both d_{\parallel} and K_{eff} have significant impacts on the spin textures of $\text{MnTe}_2/\text{ZrS}_2$. To describe their joint effect, we introduce a dimensionless parameter κ , which can be written as [37-39]:

$$\kappa = \left(\frac{4}{\pi}\right)^2 \frac{2JK_{\text{eff}}}{3d_{\parallel}^2}$$

The spin texture diagram of $\text{MnTe}_2/\text{ZrS}_2$ described by κ is illustrated in **Fig. 4(b)**. Clearly, when $|\kappa| < 1$, labyrinth domain phase can be formed. For the spin textures around $|\kappa| = 1$, magnetic skyrmion appears close to the labyrinth domains. As $|\kappa|$ increases larger than 1, the size of labyrinth domain becomes larger, and the magnetic bimeron is observed. And with increasing $|\kappa|$, the magnetic skyrmion/bimeron moves further from the labyrinth domains, and the density and radius of magnetic skyrmion/bimeron decrease. When $|\kappa| \gg 1$, both magnetic skyrmion/bimeron and labyrinth domain decay into FM pattern, leading to the trivial FM phase; see **Fig. 4(b)**. It is important to stress that the dimensionless parameter κ is only employed for describing physics of magnetic skyrmion in previous works [17,22], we show that it is also applicable for characterizing the cases of magnetic bimeron.

Conclusion

To summarize, we report the identification of multiple topological magnetism of magnetic skyrmion and bimeron in $\text{MnTe}_2/\text{ZrS}_2$ on the basis of first-principles calculations and Monte-Carlo simulations. Because of the strong interlayer hopping, this system presents a large DMI. The competition between the DMI and FM exchange interaction forms the spontaneous zero-field magnetic skyrmion in $\text{MnTe}_2/\text{ZrS}_2$. By introducing a tiny magnetic field of ~ 75 mT, skyrmion phase consisting of sub-10 nm magnetic skyrmions can be observed. Meanwhile, with including a small electric field, magnetic bimeron can be realized. This leads to the multiple topological magnetism in $\text{MnTe}_2/\text{ZrS}_2$. Moreover, through interlayer sliding, both topological spin textures can be switched off. Additionally, the roles of d_{\parallel} and K_{eff} on these spin textures are discussed, and a dimensionless parameter κ is adopt to characterize their joint effect.

Acknowledgement

This work is supported by the National Natural Science Foundation of China (Nos. 12274261 and 12074217), Shandong Provincial Science Foundation for Excellent Young Scholars (No. ZR2020YQ04), Shandong Provincial Natural Science Foundation (Nos. ZR2019QA011), Shandong Provincial Key Research and Development Program (Major Scientific and Technological Innovation Project) (No. 2019JZZY010302), Shandong Provincial QingChuang Technology Support Plan (No. 2021KJ002), and Qilu Young Scholar Program of Shandong University.

Data Availability

The data that support the findings of this study are available within this article and its supplementary material.

Reference

- [1] Mühlbauer, S., Binz, B., Jonietz, F., Pfleiderer, C., Rosch, A., Neubauer, A., Georgii, R. and Böni, P., Skyrmion lattice in a chiral magnet. *Science* 323, 915 (2009).
- [2] Yu, X.Z., Onose, Y., Kanazawa, N., Park, J.H., Han, J.H., Matsui, Y., Nagaosa, N. and Tokura, Y., Real-space observation of a two-dimensional skyrmion crystal. *Nature* 465, 901 (2010).
- [3] Bogdanov, A.N. and Panagopoulos, C., Physical foundations and basic properties of magnetic skyrmions. *Nat. Rev. Phys.* 2, 492 (2020).
- [4] Fert, A., Reyren, N. and Cros, V., Magnetic skyrmions: advances in physics and potential applications. *Nat. Rev. Mater.* 2, 1 (2017).
- [5] Göbel, B., Mertig, I. and Tretiakov, O.A., Beyond skyrmions: Review and perspectives of alternative magnetic quasiparticles. *Phys. Rep.* 895, 1 (2021).
- [6] Soumyanarayanan, A., Raju, M., Gonzalez Oyarce, A.L., Tan, A.K., Im, M.Y., Petrović, A.P., Ho, P., Khoo, K.H., Tran, M., Gan, C.K. and Ernult, F., Tunable room-temperature magnetic skyrmions in Ir/Fe/Co/Pt multilayers. *Nat. Mater.* 16, 898 (2017).
- [7] Nagaosa, N. and Tokura, Y., Topological properties and dynamics of magnetic skyrmions. *Nat. Nanotechnol.* 8, 899 (2013).
- [8] Wiesendanger, R., Nanoscale magnetic skyrmions in metallic films and multilayers: a new twist for spintronics. *Nat. Rev. Mater.* 1, 1 (2016).
- [9] Kharkov, Y.A., Sushkov, O.P. and Mostovoy, M., Bound states of skyrmions and merons near the Lifshitz point. *Phys. Rev. Lett.* 119, 207201 (2017).
- [10] Komineas, S., Rotating vortex dipoles in ferromagnets. *Phys. Rev. Lett.* 99, 117202 (2007).
- [11] Göbel, B., Mook, A., Henk, J., Mertig, I. and Tretiakov, O.A., Magnetic bimerons as skyrmion analogues in in-plane magnets. *Phys. Rev. B* 99, 060407 (2019).
- [12] Wu, Y., Zhang, S., Zhang, J., Wang, W., Zhu, Y.L., Hu, J., Yin, G., Wong, K., Fang, C., Wan, C. and Han, X., Néel-type skyrmion in $\text{WTe}_2/\text{Fe}_3\text{GeTe}_2$ van der Waals heterostructure. *Nat. Commun.* 11, 1 (2020).
- [13] Xu, C., Chen, P., Tan, H., Yang, Y., Xiang, H. and Bellaiche, L., Electric-field switching of magnetic topological charge in type-I multiferroics. *Phys. Rev. Lett.* 125, 037203 (2020).
- [14] Cho, J., Kim, N.H., Lee, S., Kim, J.S., Lavrijsen, R., Solignac, A., Yin, Y., Han, D.S., Van Hoof, N.J., Swagten, H.J. and Koopmans, B., Thickness dependence of the interfacial Dzyaloshinskii-Moriya interaction in inversion symmetry broken systems. *Nat. Commun.* 6, 1 (2015).
- [15] Yang, H., Thiaville, A., Rohart, S., Fert, A. and Chshiev, M., Anatomy of dzyaloshinskii-moriya interaction at Co/Pt interfaces. *Phys. Rev. Lett.* 115, 267210 (2015).
- [16] Beutier, G., Collins, S.P., Dimitrova, O.V., Dmitrienko, V.E., Katsnelson, M.I., Kvashnin, Y.O., Lichtenstein, A.I., Mazurenko, V.V., Nisbet, A.G.A., Ovchinnikova, E.N. and Pincini, D., Band filling control of the Dzyaloshinskii-Moriya interaction in weakly ferromagnetic insulators. *Phys. Rev. Lett.* 119, 167201 (2017).
- [17] Liang, J., Wang, W., Du, H., Hallal, A., Garcia, K., Chshiev, M., Fert, A. and Yang, H., Very large Dzyaloshinskii-Moriya interaction in two-dimensional Janus manganese dichalcogenides and its application to realize skyrmion states. *Phys. Rev. B* 101, 184401 (2020).
- [18] Li, C.K., Yao, X.P. and Chen, G., Writing and deleting skyrmions with electric fields in a multiferroic

heterostructure. *Phys. Rev. Res.* 3, L012026 (2021).

[19] Trivedi, D.B., Turgut, G., Qin, Y., Sayyad, M.Y., Hajra, D., Howell, M., Liu, L., Yang, S., Patoary, N.H., Li, H. and Petrić, M.M., Room-Temperature Synthesis of 2D Janus Crystals and their Heterostructures. *Adv. Mater.* 32, 2006320 (2020).

[20] Guo, Y., Lin, Y., Xie, K., Yuan, B., Zhu, J., Shen, P.C., Lu, A.Y., Su, C., Shi, E., Zhang, K. and HuangFu, C., Designing artificial two-dimensional landscapes via atomic-layer substitution. *Proc. Natl Acad. Sci. USA* 118, e2106124118 (2021).

[21] Shang, J., Tang, X. and Kou, L., Two dimensional ferroelectrics: Candidate for controllable physical and chemical applications. *Wires. Comput. Mol. Sci.* 11, e1496 (2021).

[22] Cui, Q., Zhu, Y., Jiang, J., Liang, J., Yu, D., Cui, P. and Yang, H., Ferroelectrically controlled topological magnetic phase in a Janus-magnet-based multiferroic heterostructure. *Phys. Rev. Res.* 3, 043011 (2021).

[23] Xu, C., Feng, J., Prokhorenko, S., Nahas, Y., Xiang, H. and Bellaiche, L., Topological spin texture in Janus monolayers of the chromium trihalides $\text{Cr}(\text{I}, \text{X})_3$. *Phys. Rev. B* 101, 060404 (2020).

[24] Jiang, J., Liu, X., Li, R. and Mi, W., Topological spin textures in a two-dimensional $\text{MnBi}_2(\text{Se}, \text{Te})_4$ Janus material. *Appl. Phys. Lett.* 119, 072401 (2021).

[25] Du, W., Dou, K., He, Z., Dai, Y., Huang, B. and Ma, Y., Spontaneous magnetic skyrmions in single-layer CrInX_3 ($\text{X} = \text{Te}, \text{Se}$). *Nano Lett.* 22, 3440 (2022).

[26] Sun, W., Wang, W., Zang, J., Li, H., Zhang, G., Wang, J. and Cheng, Z., Manipulation of magnetic skyrmion in a 2D van der Waals heterostructure via both electric and magnetic fields. *Adv. Funct. Mater.* 31, 2104452 (2021).

[27] Fragkos, S., Pappas, P., Symeonidou, E., Panayiotatos, Y. and Dimoulas, A., Magnetic skyrmion manipulation in $\text{CrTe}_2/\text{WTe}_2$ 2D van der Waals heterostructure. *Appl. Phys. Lett.* 120, 182402 (2022).

[28] Chen, W., Zhang, J.M., Nie, Y.Z., Xia, Q.L. and Guo, G.H., Tuning magnetic properties of single-layer MnTe_2 via strain engineering. *J. Phys. Chem. Solids* 143, 109489 (2020).

[29] Anderson, P.W., Antiferromagnetism. Theory of superexchange interaction. *Phys. Rev.* 79, 350 (1950).

[30] Goodenough, J.B., Theory of the role of covalence in the perovskite-type manganites $[\text{La}, \text{M}(\text{II})]\text{MnO}_3$. *Phys. Rev.* 100, 564 (1955).

[31] Kanamori, J., Superexchange interaction and symmetry properties of electron orbitals. *J Phys. Chem. Solids* 10, 87 (1959).

[32] Fang, Y., Wu, S., Zhu, Z.Z. and Guo, G.Y., Large magneto-optical effects and magnetic anisotropy energy in two-dimensional $\text{Cr}_2\text{Ge}_2\text{Te}_6$. *Phys. Rev. B* 98, 125416 (2018).

[33] Kim, J., Kim, K.W., Kim, B., Kang, C.J., Shin, D., Lee, S.H., Min, B.C. and Park, N., Exploitable magnetic anisotropy of the two-dimensional magnet CrI_3 . *Nano Lett.* 20, 929 (2019).

[34] Moriya, T., Anisotropic superexchange interaction and weak ferromagnetism. *Phys. Rev.* 120, 91 (1960).

[35] Fert, A. and Levy, P.M., Role of anisotropic exchange interactions in determining the properties of spin-glasses. *Phys. Rev. Lett.* 44, 1538 (1980).

[36] Berg, B. and Lüscher, M., Definition and statistical distributions of a topological number in the lattice $\text{O}(3)$ σ -model. *Nuclear Phys. B* 190, 412 (1981).

[37] Jia, H., Zimmermann, B. and Blügel, S., First-principles investigation of chiral magnetic properties in multilayers: $\text{Rh}/\text{Co}/\text{Pt}$ and $\text{Pd}/\text{Co}/\text{Pt}$. *Phys. Rev. B* 98, 144427 (2018).

- [38] Rohart, S. and Thiaville, A., Skyrmion confinement in ultrathin film nanostructures in the presence of Dzyaloshinskii-Moriya interaction. *Phys. Rev. B* 88, 184422 (2013).
- [39] Leonov, A.O., Monchesky, T.L., Romming, N., Kubetzka, A., Bogdanov, A.N. and Wiesendanger, R., The properties of isolated chiral skyrmions in thin magnetic films. *New J. Phys.* 18, 065003 (2016).